

Dichroism in time-resolved ARPES and valence band orbital nature in BaNiS₂

Jiuxiang Zhang^{1*}, Zhesheng Chen¹, Jonathan Caillaux¹, Yannick Klein², Andrea Gauzzi², Azzedine Bendounan³, Amina Taleb-Ibrahimi³, Luca Perfetti⁴, Evangelos Papalazarou¹ and Marino Marsi^{1*}

^{1*}Université Paris-Saclay, CNRS, Laboratoire de Physique des Solides, 91405, Orsay, France.

²Sorbonne Université, CNRS, IMPMC, IRD, MNHN, 75252, Paris, France.

³Synchrotron SOLEIL, 91192, Gif-sur-Yvette, France.

⁴Ecole Polytechnique, Institut Polytechnique de Paris, CEA/DRF/IRAMIS, CNRS, Laboratoire des Solides Irradiés, 91128, Palaiseau, France.

*Corresponding author(s). E-mail(s):

jiuxiang.zhang@universite-paris-saclay.fr;
marino.marsi@universite-paris-saclay.fr;

Abstract

Time-resolved ARPES gives access to the band structure and ultrafast dynamics of excited electronic states in solids. The orbital character of the bands close to the Fermi level is essential to understand the origin of several exotic phenomena in quantum materials. By performing polarization dependent time- and angle-resolved photoemission spectroscopy and by analyzing the chirality of the photoelectron yield for two different crystal orientations, we identify the orbital character of bands below and above the chemical potential for the Dirac semimetal **BaNiS₂**. Our results illustrate how the control and understanding of matrix elements effects in time-resolved photoemission spectroscopy can be a powerful tool for the study of quantum materials.

Keywords: Time-resolved ARPES, **BaNiS₂**, Dirac semimetal, Dichroism

1 Introduction

BaNiS₂ has recently generated increasing attention because of its peculiar properties related to the combined effects of crystal field and strong spin-orbit coupling [1–3], resulting in hidden Rashba-split spin-polarized bands. Furthermore, the presence of tunable quasi two-dimensional Dirac cones stemming from a nonsymmorphic symmetry of the lattice has been recently demonstrated [4]. It has been shown that the tunability of Dirac cones originates from the charge transfer generated by the hybridization between *p* and *d* orbitals [5], which makes BaNiS₂ a promising system to functionalize Dirac states by manipulating the strength of electron correlations. Furthermore, BaNiS₂ is the metallic precursor of BaCo_{1-x}Ni_xS₂, which presents great similarities with high-T_c cuprates, but no superconductivity [6–8]. Understanding electron-electron correlations will help obtain further insight about all these peculiar properties. In Fig. 1(a)(b), we show the crystal structure of BaNiS₂ [9] and in Fig. 1(c) the two-dimensional projection of its Brillouin zone.

The advent of time and angle-resolved photoemission spectroscopy (time-resolved ARPES) makes it possible to explore empty electronic states and their ultrafast dynamics [10], extending to the study of excited states the distinctive features of ARPES. This technique provides a direct way towards the studies of band structure of crystalline solids, and to the effects of electron-electron correlations [11]. In photoelectron spectroscopy, electrons in solids can be excited into the vacuum when they absorb photons with energy larger than the work function – an extension of the photoelectric effect. A spectrum measured with this technique contains information on the momentum and kinetic energy of photoelectrons; the intensity of the yield is proportional to the overlap integral between an initial state wave function Ψ_i transformed according to the interaction operator H_{int} and the final state wave function Ψ_f , and depends on the geometry of the experimental setup, the photon energy and the polarization of light [11–13], which can be written as following:

$$Intensity \propto |M_{fi}^k|^2 \quad (1)$$

$$M_{fi}^k = \langle \Psi_f^k | H_{int} | \Psi_i^k \rangle \propto \langle \Psi_f^k | \mathbf{A} \cdot \mathbf{p} | \Psi_i^k \rangle \quad (2)$$

where \mathbf{A} is the electromagnetic vector potential, and \mathbf{p} is the electronic momentum operator.

Having a better understanding of the relation between photoemission and spectral functions is crucial to extract more information on the electronic states, beyond the band structure $E = E(k)$, such as for instance band degeneracy and correlations. Furthermore, the photoelectron yield presents additional modulations in its intensity coming from matrix element effects [14]. The selection rules stemming from these effects can be actually exploited to obtain information on the orbital nature of the initial state by controlling some parameters used in the measurement [15–19], either suppressing or emphasizing the photoelectron yield from specific electronic states.

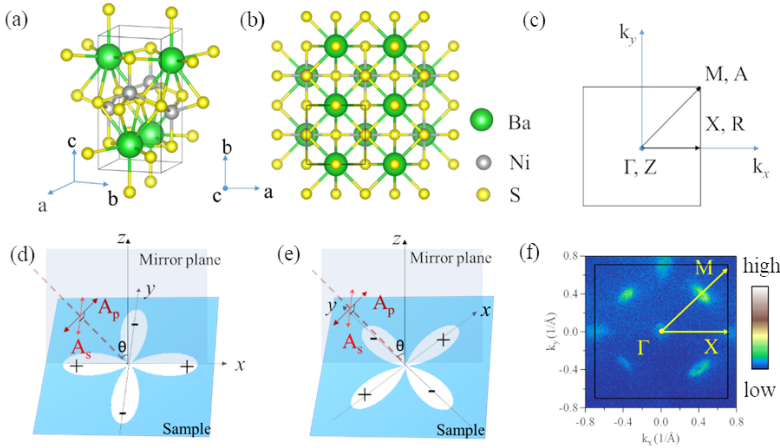


Fig. 1 (a) 3-dimensional view of the unit cell. (b) Top view of 2×2 unit cells. (c) (2D) projection of the Brillouin zone in the k_x, k_y plane. (d) Illustration of the spatial symmetry of $d_{x^2-y^2}$ with respect to the mirror plane in ΓX configuration. (e) The same but in ΓM configuration. (f) Fermi surface of BaNiS₂ acquired with 70 eV photon energy

Selection rules state that since the final state is an even function with respect to the mirror plane (we assume that the photoelectron energy analyzer is in the mirror plane), orbitals that are odd (even) with respect to the mirror plane can be detected only with light polarization that has the same parity with respect to that plane. Here we use $d_{x^2-y^2}$ as example. Fig. 1(d)(e) shows the experimental geometry. In our geometry, a photon with p polarization has an incoming electric field that lies within mirror plane, while an s polarized photon has an electric field perpendicular to the mirror plane, i.e., parallel to the sample surface: as a result, p polarization is even while s polarization is odd with respect to the mirror plane. A $d_{x^2-y^2}$ orbital has even parity when its xz plane coincides with the mirror plane, therefore it can be detected with p polarization light. The overall matrix elements for d orbitals when the mirror plane is aligned with two high symmetry directions of the crystal are summarized in Table 1. By using state of the art electron analyzers, e.g., Angle Resolved Time-of-Flight (ARTOF) analyzers, one can simultaneously measure E , k_x and k_y without rotating the sample, making it possible to discriminate between matrix element and experimental geometry effects. By combining the rotation of the crystal and the control of light polarization, one can get a clear and unambiguous relation between the modulation of the photoemission intensity and the orbital characters.

In this work, we use polarization dependent pump-probe ARPES to study the orbital character of the filled and excited electronic states of the Dirac semimetal BaNiS₂. This information is obtained thanks to detailed measurements with well-chosen crystal orientations and different light polarizations and by comparing the results with theoretical electronic band calculations.

Table 1 Possibility of detecting 3d orbitals along two high symmetry directions with p and s polarization light

High symmetry direction	Light polarization	3d orbitals				
		$d_{x^2-y^2}$	d_{z^2}	d_{xz}	d_{yz}	d_{xy}
ΓM	p	No	Yes	Yes	Yes	Yes
	s	Yes	No	Yes	Yes	No
ΓX	p	Yes	Yes	Yes	No	No
	s	No	No	No	Yes	Yes

2 Experimental methods

High quality single crystals of BaNiS₂ were grown by a self-flux method [20], and the fresh surfaces were obtained by cleaving *in-situ* along the (001) plane under ultrahigh vacuum, at a base pressure of 2×10^{-10} mbar. The time-resolved ARPES experiments were performed at 85 K using a Scienta Omicron ARTOF-2 analyzer and a femtosecond Ti:Sapphire laser system FemtoSource XL 300. The near infrared pulses (1.55 eV) were upconverted to 6.2 eV, an energy sufficient to excite photoelectrons [21], and cascade frequency mixing in $\beta - \text{BaB}_2\text{O}_4$ non-linear crystals and optics [22]. Complementary measurements have been performed on the FemtoARPES setup and on the TEMPO beamline at the SOLEIL synchrotron.

The experimental geometry for the ARPES measurements is shown in Fig. 1(d)(e). For sake of simplicity, when the sample's ΓX (ΓM) direction is in the mirror plane, we call it ΓX (ΓM) configuration, respectively. Various light polarization configurations were used during the measurements. Besides linearly polarized s and p photons (Fig. 1(d)(e)), we also used left and right circularly polarized photons generated by using a quarter-wave plate.

3 Results and discussion

The data presented in Fig. 1(f) show the Fermi surface of BaNiS₂ with reference to the indicated high symmetry directions in the a-b plane. It is possible to see the Fermi surface over the whole BZ, featuring four Dirac nodes along ΓM , four oval pockets at X and one pocket at the Γ point. The data were obtained with synchrotron radiation at 70 eV photon energy and at 80 K.

As underlined by recent studies [4–6], the most important electronic properties of BaNiS₂ are related to the Dirac cones and to the electron pocket at Γ . We consequently focused on these bands when exploring in detail the polarization dependence of the whole angular photoemission yield, by using the ARTOF photoelectron detector of our ultrafast time-resolved ARPES setup.

Fig. 2 (Fig. 3) shows photoemission data taken around Γ in ΓM (ΓX) configuration, respectively. The data taken with s polarization are presented in the upper panels, while lower panels show the corresponding spectra taken in p polarization, respectively. Three bands can be resolved in Fig. 2 and Fig. 3:

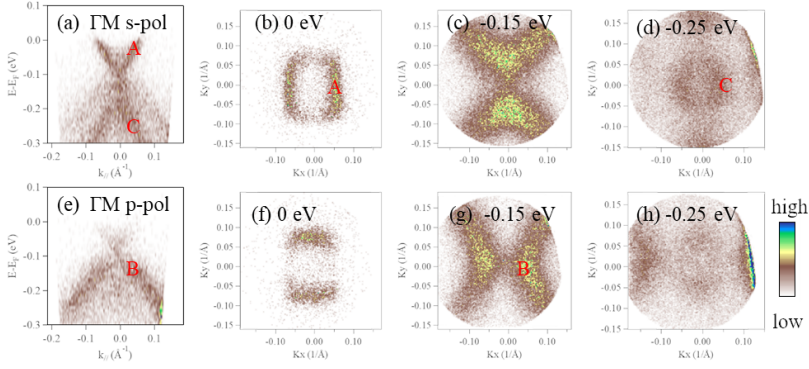


Fig. 2 ARPES in Γ M configuration. (a) $E-k$ cut with s polarization. (b)-(d) CECs with s polarization at $E-E_F = 0$ eV, -0.15 eV and -0.25 eV, respectively. (e) $E-k$ cut with p polarization. (f)-(h) CECs with p polarization at $E-E_F = 0$ eV, -0.15 eV and -0.25 eV, respectively.

one electron-like band A, two hole-like bands B and C. All three bands undergo very strong intensity variations when the light polarization is changed.

From the $E-k$ plots (Figs. 2(a) and 3(a)) we can see that both bands A and C appear intense in s polarization in Γ M configuration and in p polarization in Γ X configuration, while they cannot be observed in p polarization in Γ M configuration and in s polarization in Γ X configuration. This means that the orbital character in these two bands is even with respect to mirror plane in Γ X configuration and odd with respect to mirror plane in Γ M configuration, which point to the $d_{x^2-y^2}$ orbital character based on Table 1. This result is consistent with the study of Santos-Cottin et al. [1]. Note that both band A and band C have square shapes in constant energy contours (CECs) at selected energies $E-E_F = 0$ eV and $E-E_F = -0.25$ eV, as shown in Fig. 2(b,f) and Fig. 3(b,f), but the orientation of two bands has 45-degree difference. The band B shows opposite behaviors, as it can be observed in p polarization in Γ M configuration and in s polarization in Γ X configuration (Figs. 2(a) and 3(a)). Therefore, the orbital character is even with respect to mirror plane in Γ M configuration and odd with respect to mirror plane in Γ X configuration, which could be attributed to d_{xy} orbital character according to Table 1.

It should be emphasized that these conclusions can be extended to the empty electronic states that we have been able to access by optically pumping the system during the time-resolved ARPES measurements. In Fig. 4 we present pump-probe ARPES data at a delay where we have maximum counts above Fermi level (Fig. 4(e)) and the relative linear dichroism contrast for CEC at $E-E_F = +0.05$ eV.

From ARPES data we could see that the electron pocket A and hole pocket C have square shapes in CECs, and from the crystal structure we could know that Ni atoms are surrounded by two pyramids, one formed by S atoms, and the other formed by Ba atoms (see Fig. 1). These two pyramids have a 45-degree difference in real space, and interestingly, the two bands A and C point at

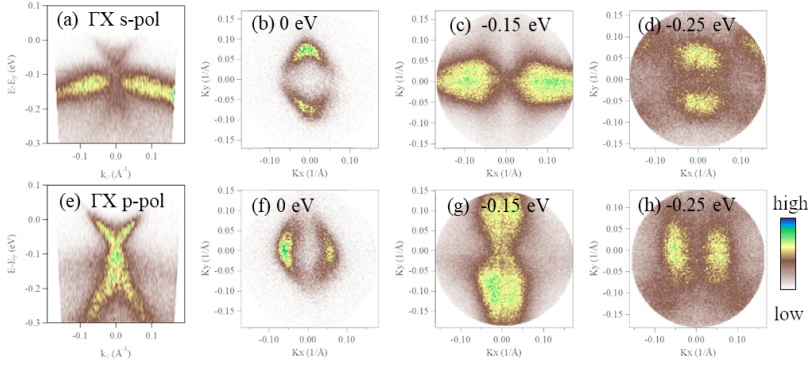


Fig. 3 ARPES in ΓX configuration. (a) $E - k$ cut with s polarization. (b)-(d) CECs with s polarization at $E - E_F = 0$ eV, -0.15 eV and -0.25 eV, respectively. (e) $E - k$ cut with p polarization. (f)-(h) CECs with p polarization at $E - E_F = 0$ eV, -0.15 eV and -0.25 eV, respectively.

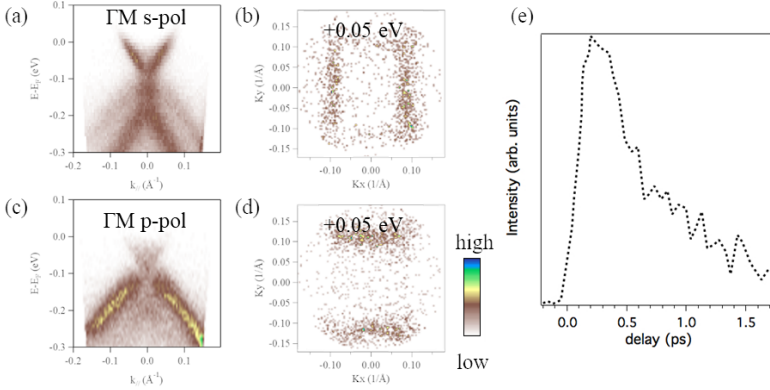


Fig. 4 Pump-probe ARPES along ΓM at a delay of 250 fs (a) $E - k$ cut with s polarization. (b) CECs with s polarization at $E - E_F = +0.05$ eV. (c) $E - k$ cut with p polarization. (d) CECs with p polarization at $E - E_F = +0.05$ eV. (e) Time evolution of the intensity of the photoelectron yield above the chemical potential

two directions with 45-degree difference. This naturally indicates a correlation between the directions of d-bands A and C, essentially, and the position of the S and Ba atoms with respect to the Ni atom.

With our 6.2 eV photon energy and manipulator rotation angle, we could reach the Dirac cone by changing the polar angle in ΓM configuration. Fig. 5 shows the polarization-dependent data around one of the Dirac nodes. We could see that in p polarization only the left branch was observed while in s polarization both branches show up with different intensities, therefore the left should be dominated by d_{z^2} orbital with some trace of $d_{x^2-y^2}$ orbital and the right branch should be attributed to $d_{x^2-y^2}$. This is consistent to what we observed in ref. [1, 5].

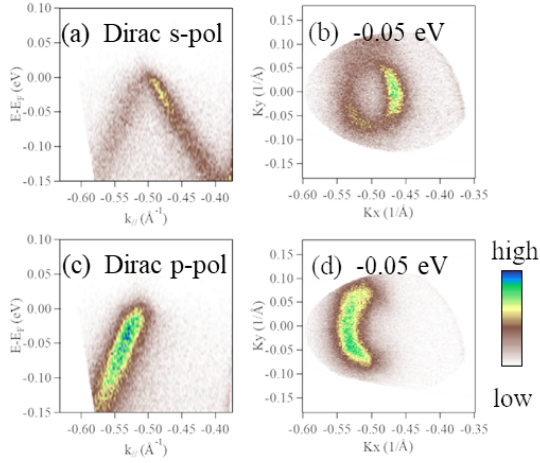


Fig. 5 ARPES of Dirac cone states. (a) $E - k$ plot with s polarization. (b) The CEC measured with s polarization at $E - E_F = -0.05$ eV. (c) $E - k$ plot with p polarization. (d) The CEC measured with p polarization at $E - E_F = -0.05$ eV.

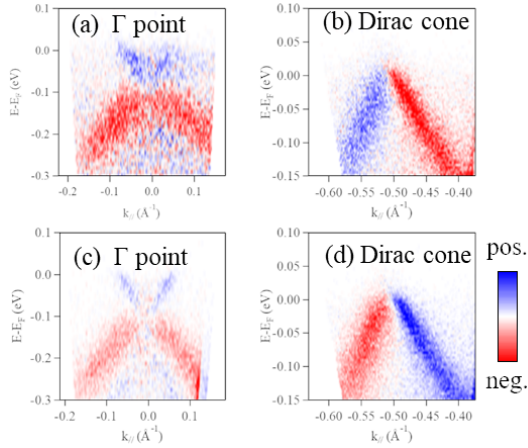


Fig. 6 Comparison between difference data taken with (a) CL and CR polarization around Γ point. (b) CL and CR polarization around Dirac cone. (c) s and p polarization around Γ point. (d) s and p polarization around Dirac cone.

Circular Dichroisms (CDs) of BaNiS₂ around Γ point and Dirac cone were investigated and plotted in Fig. 6(a)(b). The data were obtained in Γ M configuration. The CD we showed here were defined as:

$$I_{CD} = I_{CL}/I_{max1} - I_{CR}/I_{max2} \quad (3)$$

where I_{max1} and I_{max2} are the maximum of I_{CL} and I_{CR} , respectively. We can see that there were strong CD in B bands around Γ point and Dirac cone. Even though the formation mechanism of Dirac cone in BaNiS₂ is different from topological insulators [5], it shows a similar CD pattern compared to

well-known topological insulators like Bi₂Se₃ [23, 24]. In Fig. 6(c)(d) we plot the difference data between s and p polarization for comparison. It shows that around Γ point the linear and circular dichroism patterns have remarkable similarity, while around Dirac cone the linear and circular dichroism patterns are reversed, which strongly suggests that also the circular dichroism is related to the orbital nature of the bands.

4 Conclusions

We investigated the orbital character of BaNiS₂ by using time-resolved ARPES with various light polarizations and for two crystal orientations with respect to the measurement geometry. By applying the selection rules, we determined the orbital characters of three bands around Γ and two branches of Dirac cones which are located in the ΓM direction. Our data indicate that the three bands A, B and C around Γ point consist of $d_{x^2-y^2}$, d_{xy} and $d_{x^2-y^2}$ orbitals, respectively; whereas the Dirac cones in ΓM direction have a d_{z^2} and $d_{x^2-y^2}$ character. Our results demonstrate that dichroism in the time-resolved ARPES yield can be a valuable tool to investigate the orbital nature of filled and photoexcited electronic states in quantum materials.

Acknowledgements

M.M., L.P. and E.P. work was supported by "Investissement d'avenir Labex Palm" (Grant No. ANR-10-LABX-0039-PALM, by the Région Ile-de-France and in part by the France Berkeley Fund. J. Z. thanks the China Scholarship Council (CSC) for the financial support.

References

- [1] D. Santos-Cottin, M. Casula, G. Lantz, Y. Klein, L. Petaccia, P. Le Fèvre, F. Bertran, E. Papalazarou, M. Marsi, A. Gauzzi, Rashba coupling amplification by a staggered crystal field, Nat. Commun. 7 (2016) 11258.
- [2] J. Ślawińska, A. Narayan, S. Picozzi, Hidden spin polarization in nonmagnetic centrosymmetric BaNiS₂ crystal: Signatures from first principles, Phys. Rev. B 94 (2016) 241114.
- [3] L. Yuan, Q. Liu, X. Zhang, J.W. Luo, S.S. Li, A. Zunger, Uncovering and tailoring hidden Rashba spin-orbit splitting in centrosymmetric crystals, Nat. Commun. 10 (2019) 906.
- [4] N. Nilforoushan, M. Casula, M. Caputo, E. Papalazarou, J. Caillaux, Z. Chen, L. Perfetti, A. Amaricci, D. Santos-Cottin, Y. Klein, A. Gauzzi, M. Marsi, Photoinduced renormalization and electronic screening of quasi-two-dimensional Dirac states in BaNiS₂, Phys. Rev. Res. 2 (2020) 043397.

- [5] N. Nilforoushan, M. Casula, A. Amaricci, M. Caputo, J. Caillaux, L. Khalil, E. Papalazarou, P. Simon, L. Perfetti, I. Vobornik, P.K. Das, J. Fujii, A. Barinov, D. Santos-Cottin, Y. Klein, M. Fabrizio, A. Gauzzi, M. Marsi, Moving Dirac nodes by chemical substitution, *Proc. Natl. Acad. Sci. U. S. A.* 118 (2021) e2108617118.
- [6] D. Santos-Cottin, A. Gauzzi, M. Verseils, B. Baptiste, G. Feve, V. Freulon, B. Plaçais, M. Casula, Y. Klein, Anomalous metallic state in quasi-two-dimensional BaNiS₂, *Phys. Rev. B.* 93 (2016) 125120 .
- [7] B. Mansart, V. Brouet, E. Papalazarou, M. Fuglsang Jensen, L. Petaccia, S. Gorovikov, A.N. Grum-Grzhimailo, F. Rullier-Albenque, A. Forget, D. Colson, M. Marsi, Orbital nature of the hole-like Fermi surface in superconducting Ba(Fe_{1-x}Co_x)₂As₂, *Phys. Rev. B* 83 (2011) 064516.
- [8] V. Brouet, M.F. Jensen, P.H. Lin, A. Taleb-Ibrahimi, P. Le Fèvre, F. Bertran, C.H. Lin, W. Ku, A. Forget, D. Colson, Impact of the two Fe unit cell on the electronic structure measured by ARPES in iron pnictides, *Phys. Rev. B* 86 (2012) 075123 .
- [9] I.E. Grey, H. Steinfink, Crystal Structure and Properties of Barium Nickel Sulfide, a Square-Pyramidal Nickel (II) Compound, *J. Am. Chem. Soc.* 92 (1970) 5093–5095.
- [10] M. Marsi, Ultrafast electron dynamics in topological insulators, *Phys. Status Solidi RRL* 12 (2018) 1800228.
- [11] A. Damascelli, Z. Hussain, Z.X. Shen, Angle-resolved photoemission studies of the cuprate superconductors, *Rev. Mod. Phys.* 75 (2003) 473–541.
- [12] A. Damascelli, Probing the electronic structure of complex systems by ARPES, *Phys. Scr. T.* T109 (2004) 61–74.
- [13] J.A. Sobota, Y. He, Z.X. Shen, Angle-resolved photoemission studies of quantum materials, *Rev. Mod. Phys.* 93 (2021) 1–72.
- [14] M. Lindroos, S. Sahrakorpi, A. Bansil, Matrix element effects in angle-resolved photoemission from Bi₂Sr₂CaCu₂O₈ Energy and polarization dependencies, final state spectrum, spectral signatures of specific transitions, and related issues, *Phys. Rev. B* 65 (2002) 054514.
- [15] S. Beaulieu, M. Schüler, J. Schusser, S. Dong, T. Pincelli, J. Maklar, A. Neef, F. Reinert, M. Wolf, L. Rettig, J. Minár, R. Ernstorfer, Unveiling the orbital texture of 1T – TiTe₂ using intrinsic linear dichroism in multidimensional photoemission spectroscopy, *Npj Quantum Mater.* 6 (2021) 93.

- [16] F. Chen, Q.Q. Ge, M. Xu, Y. Zhang, X.P. Shen, W. Li, M. Matsunami, S. ichi Kimura, J.P. Hu, D.L. Feng, The orbital characters of low-energy electronic structure in iron-chalcogenide superconductor $K_xFe_{2-y}Se_2$, Chinese Sci. Bull. 57 (2012) 3829–3835.
- [17] X.P. Wang, P. Richard, Y.B. Huang, H. Miao, L. Cevey, N. Xu, Y.J. Sun, T. Qian, Y.M. Xu, M. Shi, J.P. Hu, X. Dai, H. Ding, Orbital characters determined from Fermi surface intensity patterns using angle-resolved photoemission spectroscopy, Phys. Rev. B 85 (2012) 214518.
- [18] E. Papalazarou, M. Gatti, M. Marsi, V. Brouet, F. Iori, L. Reining, E. Annese, I. Vobornik, F. Offi, A. Fondacaro, S. Huotari, P. Lacovig, O. Tjernberg, N.B. Brookes, M. Sacchi, P. Metcalf and G. Panaccione, Valence band electronic structure of V_2O_3 : identification of V and O bands , Phys. Rev. B 80 (2009) 155115.
- [19] Y. Ohtsubo, J. Mauchain, J. Faure, E. Papalazarou, M. Marsi, P. Le Fèvre, F. Bertran, A. Taleb-Ibrahimi, and L. Perfetti, Giant Anisotropy of Spin-Orbit Splitting at the Bismuth Surface , Phys. Rev. Lett. 109 (2012) 226404.
- [20] S. Shamoto, S. Tanaka, E. Ueda, M. Sato, Single crystal growth of BaNiS₂, J. Cryst. Growth. 154 (1995) 197–201.
- [21] M. Marsi, M. Trovo, R.P. Walker, L. Giannessi, G. Dattoli, A. Gatto, N. Kaiser, S. Gunster, D. Ristau, M.E. Couprie, D. Garzella, J.A. Clarke, M.W. Poole, Operation and performance of a free electron laser oscillator down to 190 nm, Appl. Phys. Lett. 80 (2002) 2851–2853.
- [22] A. Gatto, R. Thielsch, J. Heber, N. Kaiser, D. Ristau, S. Gunster, J. Kohlhaas, M. Marsi, M. Trovo, R.P. Walker, D. Garzella, M.E. Couprie, P. Torchio, M. Alvisi, C. Amra, High performance deep-ultraviolet optics for free-electron laser, Appl. Optics 41 (2002) 3236–3241.
- [23] J. Zhang, J. Caillaux, Z. Chen, M. Konczykowski, A. Hruban, Probing spin chirality of photoexcited topological insulators with circular dichroism: multi-dimensional time-resolved ARPES on Bi_2Te_2Se and Bi_2Se_3 , 253 (2021) 147125.
- [24] S.R. Park, J. Han, C. Kim, Y.Y. Koh, C. Kim, H. Lee, H.J. Choi, J.H. Han, K.D. Lee, N.J. Hur, M. Arita, K. Shimada, H. Namatame, M. Taniguchi, Chiral orbital-angular momentum in the surface states of Bi_2Se_3 , Phys. Rev. Lett. 108 (2012) 046805.